J|A|C|S
ARTICLES
Published on Web 10/16/2004

Key Role of Electrostatic Interactions in Bacteriorhodopsin Proton Transfer

Ana-Nicoleta Bondar,*[,†,‡] Stefan Fischer,[†] Jeremy C. Smith,[†] Marcus Elstner,[‡,§] and Sándor Suhai*[,‡]

Contribution from the Computational Molecular Biophysics, IWR, Heidelberg University, Im Neuenheimer Feld 368, Heidelberg, Germany; Molecular Biophysics Department, German Cancer Research Center, Im Neuenheimer Feld 580, D-69120 Heidelberg, Germany; and Theoretische Physik, University of Paderborn, Warburger Strasse 100, 33098 Paderborn, Germany

Received April 7, 2004; E-mail: nicoleta.bondar@iwr.uni-heidelberg.de; S.Suhai@dkfz-heidelberg.de

Abstract: The first proton transport step following photon absorption in bacteriorhodopsin is from the 13-cis retinal Schiff base to Asp85. Configurational and energetic determinants of this step are investigated here by performing quantum mechanical/molecular mechanical minimum-energy reaction-path calculations. The results suggest that retinal can pump protons when in the 13-cis, 15-anti conformation but not when 13-cis, 15-syn. Decomposition of the proton transfer energy profiles for various possible pathways reveals a conflict between the effect of the intrinsic proton affinities of the Schiff base and Asp85, which favors the neutral, product state (i.e., with Asp85 protonated), with the mainly electrostatic interaction between the protein environment with the reacting partners, which favors the ion pair reactant state (i.e., with retinal protonated). The rate-limiting proton-transfer barrier depends both on the relative orientations of the proton donor and acceptor groups and on the pathway followed by the proton; depending on these factors, the barrier may arise from breaking and forming of hydrogen bonds involving the Schiff base, Asp85, Asp212, and water w402, and from nonbonded interactions involving protein groups that respond to the charge rearrangements in the Schiff base region.

Introduction

Proton transfer plays a crucial role in biological processes, such as enzyme catalysis and the creation of proton gradients by membrane-bound proteins. A well-studied example of the latter type of system is bacteriorhodopsin, a light-driven proton pump found in the purple membrane of the archeabacterium *Halobacterium salinarium* (for recent reviews, see refs 1−3). Bacteriorhodopsin is a seven-helix membrane protein to which a retinal chromophore is covalently bound via a protonated Schiff base. Due to its relatively small size and high stability, bacteriorhodopsin is an excellent model system for cellular ion pumps. The absorption of one photon triggers a photocycle comprising an initial isomerization of the retinal chromophore followed by five proton transport steps. The net effect of one cycle is the transport of one proton from the cytoplasmic to the extracellular side of the membrane. The absorbed light energy is thus converted into an electrochemical gradient that is used by the cell to synthesize adenosine triphosphate (ATP). Understanding the atomic-detail mechanism of proton transport in bacteriorhodopsin and how it is coupled to conformational change should provide valuable insight into physical mechanisms of active transport in biology.

Perhaps the best characterized proton transfer step is the first one, from the Schiff base to Asp85 over a ∼4 Å distance. This transfer occurs between the L and M states of the bacteriorhodopsin photocycle. The L intermediate forms through the decay of the previous, photoisomerized K state, and it itself decays into M on a ∼10 μs time scale.[4] The atomic-detail mechanism by which the first proton transfer step occurs is not completely understood due to difficulties in experimentally characterizing the associated transition state(s) required to define reaction mechanisms. Based on X-ray crystallography, Fourier transform infrared (FTIR) spectroscopy, and site-directed mutagenesis, several models have been proposed. The mechanism is likely to depend on whether the Schiff base NH bond orients toward the extracellular or cytoplasmic side of the protein. This orientation is the subject of debate, as also are the protocols for trapping and assigning the relevant photocycle intermediates.[3,5,6] For the retinal in the pre-proton-transfer states, both extracellular and cytoplasmic orientations of the Schiff base NH groups have

† Heidelberg University.
‡ German Cancer Research Center.
§ University of Paderborn.

(1) Subramaniam, S.; Lindahl, M.; Bullough, P.; Faruki, A. R.; Tittor, J.; Oesterhelt, D.; Brown, L.; Lanyi, J. K.; Henderson, R. *J. Mol. Biol.* **1999**, *287*, 145−161.
(2) Lanyi, J. K. *J. Phys. Chem. B.* **2000**, *104*, 11441−11448.
(3) Neutze, R.; Pebay-Peyroula, E.; Edman, K.; Royant, A.; Navarro, J.; Landau, E. M. *Biochim. Biophys. Acta* **2002**, *1565*, 144−167.
(4) Ludman, K.; Gergely, C.; Váró, G. *Biophys. J.* **1998**, *75*, 3110−3119.
(5) Balashov, S. P.; Ebrey, T. G. *Photochem. Photobiol.* **2001**, *73*, 453−462.
(6) Edman, K.; Royant, A.; Larsson, G.; Jacobson, F.; Taylor, T.; van der Spoel, D.; Landau, E. M.; Pebay-Peyroula, E.; Neutze, R. *J. Biol. Chem.* **2004**, *279*, 2147−2158.

10.1021/ja047982i CCC: $27.50

been proposed. An extracellular Schiff base orientation achieved through significant twisting of single and/or double bonds was proposed based on theoretical[7] and X-ray crystallography data.[8,9] From this retinal configuration either a direct transfer to Asp85 or water-mediated proton transfer to Asp85 is conceivable.[7,9,10] For a cytoplasmic Schiff base orientation, as has also been proposed,[6] putative proton-transfer pathways are (i) direct to Asp85,[6] (ii) via Thr89,[6,11] or (iii) via dissociation of water molecule w402 that in the initial (bR) state bridges the Schiff base with Asp85 and Asp212 via hydrogen bonds.[2,10]

Not only the preferred pathway for the first proton-transfer step must be understood, but also what triggers the proton transfer and what the molecular origin is of the associated ~10 kcal/mol energy barrier.[4] It has been suggested that particularly important events involve changes in the relative pK_a values of the donor and acceptor groups[12] due to light-induced charge separation[13] and are modulated by structural water,[14,15] hydrogen-bonding interactions,[16] the retinal isomeric state,[7,17] the donor/acceptor relative orientation and coupling to protein dielectric.[18]

Over the years, several theoretical investigations have complemented experiment by providing valuable data on the physicochemical properties of retinal, both isolated and in the protein environment.[19−24] For example, molecular dynamics (MD) simulations of increasing complexity have been performed, including a ns time scale simulation of the whole purple membrane.[25] Free energy simulations correctly predicted the presence of a chain of four water molecules connecting Asp96 to the Schiff base[26] that was only recently observed by X-ray crystallography.[27] Multiconformation continuum electrostatics analysis has demonstrated a long-range coupling between the Schiff base region and the extracellular proton release site,[28] as had been suggested from experiment.[29] Other electrostatic calculations have suggested that Thr89 may participate in a proton-transfer pathway.[30]

Theoretical investigations of possible proton-transfer pathways in bR are complicated by computer power limitations. Accurate quantum mechanical methods are required to describe proton transfer, but the quantum mechanical treatment of the whole protein (about 3000 atoms in the case of bacteriorhodopsin) would be computationally prohibitive. Instead, to simulate proton transfer in proteins, a combined quantum mechanics/molecular mechanics (QM/MM) methodology can be used. QM/MM approaches combine a quantum mechanical treatment of those protein groups that are candidates for participating in the chemical reaction with a faster, molecular mechanical description of the environment.[31−33] In recent years QM/MM approaches have been used to examine the role of the hydrogen-bonded network in the nonisomerized retinal configuration,[34] obtain insights into the structure of the K state and its decay product KL,[35,36] investigate the dynamics of proton transfer from Asp96 to the deprotonated Schiff base,[37] and understand the factors determining the absorption maxima of retinal proteins[23,38−41] and the quantum dynamics of retinal photoisomerization.[36,42]

In the present work we employ QM/MM minimum-energy path calculations to investigate the proton transfer energy profiles in bacteriorhodopsin for various retinal isomeric states. The calculations reveal that, unlike 13-cis, 15-anti, the 13-cis, 15-syn retinal state is not compatible with an active, proton pumping photocycle. Regardless of the relative orientation of the retinal Schiff base and Asp85, the proton transfer energy profiles are mainly determined by two opposite-sign contributions, one of which being the interaction between Asp85 and the 13-cis retinal, strongly favoring proton transfer, and the other arising from the protein electrostatic environment that stabilizes the ion pair state and gives rise to a proton transfer barrier.

Methods

Model System. Three main retinal isomeric states have been proposed for the isomerized, pre-proton-transfer K and L states. These are (i) 13-cis, 14-trans, 15-anti retinal, which can be oriented toward the cytoplasmic side[43,44] (Figure 1A) or, through significant twisting, toward the extracellular side of the membrane;[8,45] (ii) extracellular 13,14-dicis retinal (Figure 1B), whose existence prior to the first proton transfer step has been the subject of debate;[7,46,47] and (iii) 13-cis, 14-trans, 15-syn twisted retinal (Figure 1C), as indicated by a putative L-state structure.[9] We modeled and used for proton transfer calculations all the above retinal configurations.

As discussed in the Introduction, the structures of the bacteriorhodopsin intermediates and the corresponding chromophore configurations

(7) Schulten, K.; Tavan, P. *Nature* **1978**, *272*, 85−86.
(8) Schobert, B.; Cupp-Vickery, J.; Hornak, V.; Smith, S. O.; Lanyi, J. K. *J. Mol. Biol.* **2002**, *321*, 715−726.
(9) Lanyi, J. K.; Schobert, B. *J. Mol. Biol.* **2003**, *328*, 439−450.
(10) Luecke, H. *Biochim. Biophys. Acta* **2000**, *1460*, 133−156.
(11) Subramaniam, S.; Henderson, R. *Nature* **2000**, *406*, 653−657.
(12) Kaliski, O.; Ottolenghi, M.; Honig, B.; Korenstein, R. *Biochemistry* **1981**, *20*, 649−655.
(13) Warshel, A. *Photochem. Photobiol.* **1979**, *30*, 285−290.
(14) Hildebrandt, P.; Stockburger, M. *Biochemistry* **1984**, *23*, 5539−5548.
(15) Gat, Y.; Sheves, M. *J. Am. Chem. Soc.* **1993**, *115*, 3772−3773.
(16) Baasov, T.; Sheves, M. *Biochemistry* **1986**, *25*, 5249−5258.
(17) Sampogna, R. V.; Honig, B. *Biophys. J.* **1994**, *66*, 1341−1352.
(18) Scheiner, S.; Duan, X. *Biophys. J.* **1991**, *60*, 874−883.
(19) Honig, B.; Warshel, A.; Karplus, M. *Acc. Chem. Res.* **1975**, *8*, 92−100.
(20) Tavan, P.; Schulten, K.; Oesterhelt, D. *Biophys. J.* **1985**, *47*, 415−430.
(21) Beppu, Y.; Kakitani, T.; Tokunaga, F. *Photochem. Photbiol.* **1992**, *56*, 1113−1117.
(22) Tajkhorshid, E.; Paizs, B.; Suhai, S. *J. Phys. Chem. B* **1999**, *103*, 4518−4527.
(23) Rajamani, R.; Gao, J. *J. Comput. Chem.* **2002**, *23*, 96−105.
(24) Murata, K.; Fujii, Y.; Enomoto, N.; Hata, M.; Hoshino, T.; Tsuda, M. *Biophys. J.* **2000**, *79*, 982−991.
(25) Baudry, J.; Tajkorshid, E.; Molnar, F.; Philip, J.; Schulten, K. *J. Phys. Chem. B.* **2001**, *105*, 905−918.
(26) Roux, B.; Nina, M.; Pomès, R.; Smith, J. C. *Biophys. J.* **1996**, *71*, 670−681.
(27) Schobert, B.; Brown, L. S.; Lanyi, J. K. 2003. *J. Mol. Biol.* **2003**, *330*, 553−570.
(28) Song, Y.; Mao, J.; Gunner, M. R. *Biochemistry* **2003**, *42*, 9875−9888.
(29) Balashov, S. P.; Imasheva, E. S.; Govindjee, R.; Ebrey, T. *Biophys. J.* **1996**, *70*, 473−481.
(30) Nakajima, S.; Ohno, K.; Inoue, Y.; Sakurai, M. *J. Phys. Chem. B* **2003**, *107*, 2867−2874.
(31) Singh, U. C.; Kollman, P. *J. Comput. Chem.* **1986**, *7*, 718−730.
(32) Field, M. J.; Bash, P. A.; Karplus, M. *J. Comput. Chem.* **1990**, *11*, 700−733.
(33) Warshel, A. Computer Modeling of chemical reactions in enzymes and solutions. John Willey & Sons: New York, 1991.
(34) Hayashi, S.; Ohmine, I. *J. Phys. Chem. B* **2000**, *104*, 10678−10691.
(35) Hayashi, S.; Tajkhorshid, E.; Schulten, K. *Biophys. J.* **2002**, *83*, 1281−1297.
(36) Hayashi. S.; Tajkhorshid, E.; Schulten, K. *Biophys. J.* **2003**, *85*, 1440−1449.
(37) Lee, Y. S.; Krauss, M. *J. Am. Chem. Soc.* **2004**, *126*, 2225−2230.
(38) Hayashi, S.; Tajkhorshid, E.; Pebay-Pyroula, E.; Royant, A.; Landau, E. M.; Navarro, J.; Schulten, K. *J. Phys. Chem. B* **2001**, *105*, 10124−10131.
(39) Houjou, H.; Inoue, Y.; Sakurai, M. *J. Phys. Chem. B* **2001**, *105*, 867−879.
(40) Ferre, N.; Olivucci, M. *J. Am. Chem. Soc.* **2003**, *125*, 6868−6869.
(41) Sakurai, M.; Sakata, K.; Saito, S.; Nakajima, S.; Inoue, Y. *J. Am. Chem. Soc.* **2003**, *125*, 3108−3112.
(42) Warshel, A.; Chu, Z. T. *J. Phys. Chem. B* **2001**, *105*, 9857−9871.
(43) Edman, K.; Nollert, P.; Royant, A.; Belrhali, H.; Peyroula, E. P.; Hajdu, J.; Neutze, R.; Landau, E. M. *Nature* **1999**, *401*, 822−826.
(44) Royant, A.; Edman, K.; Ursby, T.; Peyroula, E. P.; Landau, E. M.; Neutze, R. *Nature* **2000**, *406*, 645−648.
(45) Matsui, Y.; Sakai, K.; Murakami, M.; Shiro, Y.; Adachi, S.; Okumura, H.; Kouyama, T. *J. Mol. Biol.* **2002**, *324*, 469−481.
(46) Gerwert, K.; Siebert, F. *EMBO J.* **1986**, *5*, 805−811.
(47) Fodor, S. P. A.; Ames, J. B.; Gebhard, R.; van der Berg, E. M. M.; Stoeckenius, W.; Lugtemburg, J.; Mathies, R. A. *Biochemistry* **1988**, *27*, 7097−7101.

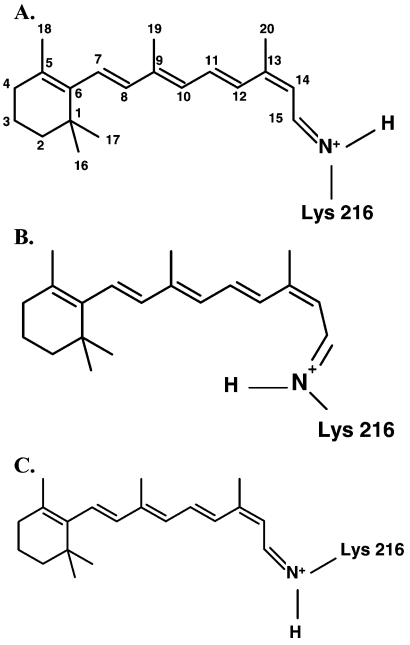

Figure 1. Different configurations of 13-cis retinal. (A) 14-trans, 15-anti; (B) 14-cis, 15-anti; (C) 14-trans, 15-syn.

are still under discussion. For example, it has been argued that the L-state structure of ref 44 was solved using a protein sample significantly contaminated with other intermediates.[5,48] Even though subtle conformational changes occurring prior to retinal deprotonation may be important for proton transfer, spectroscopic data indicate that only small global protein conformational changes take place in the first half of the photocycle.[1,49,50] Therefore, we used the K-state structure of ref 43 to model end states having 13-cis, 14-trans, 15-anti retinal. The 13,14-dicis model was obtained by applying a rigid torsion of 180° around the retinal $C_{14}-C_{15}$ single bond in the K-state structure of ref 43. The L-state structure of ref 9 was used to model retinal in the 13-cis, 15-syn configuration.

The crystal structures have several unresolved residues. The missing terminal residues are unlikely to influence the reaction mechanism under investigation and were not included. Instead, the protein was capped with neutral groups (CH_3-CO- and $-NH-CH_3$ for the N and C termini, respectively). Missing internal side chains were modeled using CHARMM.[51] The structures used in the present calculations consisted of 227 protein residues, from Thr5 to Gly231 inclusive. Hydrogen atoms not visible in the experimental structures were included using the HBUILD facility of CHARMM.[52] The calculations were performed for an isolated bacteriorhodopsin monomer.

A. Protonation States. Asp96, Asp115, and Glu204 were modeled in their uncharged form, as indicated by experiment.[53,54] Standard protonation states were assumed for the remaining protein groups.

B. Water Molecules. All water molecules present in the crystal structures were included in the calculations. The location of water molecules that can hydrogen bond to the proton donor and/or acceptor is likely to be important in determining the proton-transfer mechanism.[55] No water molecule is found in the hydrogen-bonding distance from the Schiff base in the crystal structure of ref 43. However, recent FTIR[55] and crystallographic data[8,9] indicate that in the K-, L-, and early-M-states, water w402 is in a position close to that in the bR state. Based on the above considerations, water w402 was included in all calculations.

C. Mobile Region. In all path calculations a part of the protein backbone was fixed. The subset of atoms whose coordinates were allowed to change (the mobile region) consisted of 827 atoms comprising the retinal, one layer of surrounding amino acid residues, and other water molecules and protein groups for which flexibility was suspected to be possibly coupled to proton transfer.

D. Quantum Mechanical Region. A total of 86 atoms were treated quantum mechanically. These comprise the proton donor and acceptor groups (retinal and Asp85, respectively) and other groups that might potentially serve as intermediate proton carriers: Thr89, Asp212, and w402.

E. QM/MM Frontier Bonds. The boundary dividing the quantum and classical regions was chosen at the $C_\beta-C_\gamma$ covalent bond in Lys216, as test calculations revealed that neither the geometry nor the proton affinity of retinal is affected by the link atom when placed in this position. In the cases of Thr89, Asp85, and Asp212 residues, the link atom was attached to the C_β atom. To avoid artifactual polarization of the frontier bond that can take place due to the presence of nonzero charges on the classical atom of the frontier bond,[56] the partial charge on the classical partner of the frontier bond (i.e, C_α) was set to zero.

F. Potential Energy Function. The total energy of the QM/MM system is given by

$$E = E_{QM} + E_{MM} + E_{QM/MM} \quad (1)$$

where E_{QM} describes the interaction energy of all quantum mechanical electrons and nuclei, E_{MM} describes the bonded and nonbonded interactions of the MM atoms, and $E_{QM/MM}$ gives the energy of all interactions between the quantum and classical particles.

Interactions between the classical atoms (E_{MM}) are given by the potential energy function of CHARMM[51] with the parameter set 22[57] for aromatic side chains and parameter set 19[58] for the rest of the protein. E_{MM} contains harmonic terms corresponding to bonded interactions including covalent bond stretches, valence angle bending, and improper angles. A sinusoidal dihedral angle term is also included. Lenard−Jones, van der Waals, and Coulombic terms represent the nonbonded interactions. Here, the Coulombic term was smoothly brought to zero by multiplying by a cubic switch function from 7 to 14 Å. The relative dielectric constant was set to 1. The TIP3P model was used to describe the MM water molecules.[59]

Minimization of the end states requires about 1000 energy calls each, and the calculation of a single proton transport path, about 10 000 calls. Given the computational cost, it was not possible to optimize the pathways using a high-level ab initio quantum mechanical treatment of the reaction region. The solution to this problem employed here is to use an approximate method for path optimizations that can describe bond breaking and forming with reasonable levels of accuracy and computational cost. The energy profiles of the thus calculated pathways were subsequently refined with higher-level single point calculations. The methods and basis sets used for both finding the paths and the single-point calculations were chosen based on their accuracy in describing proton transfer energies, retinal/acetate relative proton affinities, and retinal structural and torsional properties. In a QM/MM study of the proton transfer reactions in triose phosphatase isomerase, it was found that the approximate DFT method self-consistent charge density functional tight binding (SCC-DFTB[60]) agrees to within 2−4

(48) Lanyi, J. K.; Luecke, H. *Curr. Opin. Struct. Biol.* **2001**, *11*, 415−419.
(49) Hendrikson, F. M.; Burkard, F.; Glaeser, R. M. *Biophys. J.* **1998**, *75*, 1446−1454.
(50) Bullough, P. A.; Henderson, R. *J. Mol. Biol.* **1999**, *286*, 1663−1671.
(51) Brooks B. R.; Bruccoleri, R. E.; Olafson, B. D.; States, D. J.; Swaminathan, S.; Karplus, M. *J. Comput. Chem.* **1983**, *4*, 187−217.
(52) Brünger, A. T.; Karplus, M. *Proteins* **1988**, *4*, 148−156.
(53) Metz, G.; Siebert, F.; Engelhardt, M. *FEBS Lett.* **1992**, *303*, 237−241.
(54) Brown, L. S.; Sasaki, J.; Kandori, H.; Maeda, A.; Needleman, R.; Lanyi, J. K. *J. Biol. Chem.* **1995**, *270*, 27122−27126.
(55) Tanimoto, T.; Furutani, Y.; Kandori, H. *Biochemistry* **2003**, *42*, 2300−2306.
(56) Reuter, N.; Dejaegere, A.; Maigret, B.; Karplus, M. *J. Phys. Chem. A* **2000**, *104*, 1720−1735.
(57) MacKerell, A. D.; et al. *J. Phys. Chem. B* **1998**, *102*, 3586−3616.
(58) Neria, E.; Fischer S.; Karplus, M. *J. Chem. Phys.* **1996**, *105*, 1902−1921.
(59) Jorgensen, W.; Chandrasekhar, J.; Madura, J.; Impey, R.; Klein, M. *J. Chem. Phys.* **1983**, *79*, 926−935.
(60) Elstner, M.; Porezag, D.; Jungnickel, G.; Elsner, J.; Haugk, M.; Frauenheim, Th.; Suhai, S.; Seifert, G. *Phys. Rev. B.* **1998**, *58*, 7260−7268.

kcal/mol with B3LYP/6-31+G** for the proton-transfer barriers.[61] Also, for the description of the geometry and torsional barriers for retinal models, SCC-DFTB is in good agreement with B3LYP/6-31G*.[62] However, the standard SCC-DFTB differs by ~10 kcal/mol from B3LYP/6-31G** in the binding energy of a proton to a neutral nitrogen forming a cation. In the present work we use a special parametrization of the Schiff base NH bond, such that the SCC-DFTB and B3LYP/6-31G** agree to within 2 kcal/mol in describing the proton affinity of acetate relative to retinal. Moreover, the two methods agree with each other to within 1−3 kcal/mol in describing the reactant and product energy differences for the proton transfer pathways investigated here. Pursuant to these considerations it was decided to use SCC-DFTB to describe the quantum-mechanical region for the calculation of the possible proton transport pathways. Subsequently, single-point B3LYP/6-31G** energy calls were performed on the SCC-DFTB/MM-optimized pathways.

In cases such as bacteriorhodopsin, where the boundary between the QM and MM regions crosses covalent bonds, $E_{QM/MM}$ consists of a sum of bonded and nonbonded interactions:

$$E_{QM/MM} = E^{b}_{QM/MM} + E^{nb}_{QM/MM}$$

$$E^{nb}_{QM/MM} = E^{coul}_{QM/MM} + E^{vdw}_{QM/MM} \quad (2)$$

where $E^{nb}_{QM/MM}$ gives the nonbonded interactions and the bonded term $E^{b}_{QM/MM}$ ensures the correct geometrical positioning of the QM subsystem with respect to the MM part. In the hydrogen link-atom approach adopted here, the bonded terms include valence angle and dihedral angle terms that extend at most to the second quantum mechanical atom. In computing the van der Waals interactions between quantum nuclei and classical atoms ($E^{vdw}_{QM/MM}$), the QM atoms are assigned the van der Waals parameters of the MM atoms. The Coulomb interactions between the QM and MM parts ($E^{coul}_{QM/MM}$) are calculated according to the SCC-DFTB[61] and GAMESS-UK[63]/CHARMM[51] implementations.

In the Results section the E and E_{QM} energy terms are decomposed according to eqs 1 and 2. The MM interactions are decomposed as follows:

$$E_{MM} = E^{nb}_{MM} + E^{b}_{MM}$$

$$E^{nb}_{MM} = E^{coul}_{MM} + E^{vdw}_{MM} \quad (3)$$

where the superscripts "nb" and "b" denote nonbonded and bonded interactions, respectively, "coul" indicates Coulombic, and "vdw", van der Waals interactions.

The QM/MM energy profiles obtained using SCC-DFTB and B3LYP/6-31G** for the description of the QM part are denoted SCC-DFTB/MM and B3LYP/MM, respectively.

Energy Minimization. Each reactant and product state was QM/MM energy minimized using the SCC-DFTB module of CHARMM.[61] The minimizations were performed to an RMS energy gradient of 10^{-3} kcal/mol Å. During the minimizations harmonic constraints were placed on the heavy atoms and were progressively weakened, from 10 kcal/mol to 1 kcal/mol with a step size of 1 kcal/mol, and subsequently from 1 kcal/mol to zero with a step size of 0.1 kcal/mol. The QM/MM-optimized reactant states deviate by 0.5 Å relative to the starting structures (rmsd values).

Reaction Path Method. Kinetic studies of the bacteriorhodopsin photocycle indicate that enthalpy dominates the free-energy barrier of the primary proton transfer.[4] This concurs with the observation that no significant protein conformational changes occur in the first half of the photocycle.[1] Consequently, as a first approximation we can equate potential energy barriers with free energy barriers.

To compute minimum energy pathways and locate all saddle points along these pathways, we applied the Conjugate Peak Refinement algorithm (CPR[64]) as implemented in the TREK module of CHARMM. The CPR method has allowed the mechanism of several complex transitions in proteins to be understood[65] and has been combined with QM/MM in the investigation of chemical reactions.[66]

The a priori definition of a reaction coordinate is not required in CPR calculations. However, energy-minimized end states (i.e., reactant and product states) are required. Here we denote as *reactant state* (R) the state characterized by a protonated Schiff base and unprotonated Asp85. Unprotonated retinal and protonated Asp85 define the *product state* (P). In the present work we investigate only very local charge rearrangement. The larger-scale protein response to the changed charge distribution in the active site will be addressed in future calculations. Accordingly, both end states of the reaction were prepared starting from the same crystal structure. The Schiff base NH orientation in each reactant and product state is specified using the labels EC (extracellular) and CP (cytoplasmic). CP−R and CP−P1/CP−P2 denote reactant and two product states with cytoplasmic orientations of the Schiff base NH group. Similarly, the Schiff base has an extracellular orientation in the end states labeled EC−R1/EC−R2 (reactants) and EC−P (product).

Path segments between the saddle points were further refined using the synchronous chain minimization (SCM) algorithm, a "locally updated-plane" procedure[67] implemented in the TREK module. SCM minimizes path points to bring them closer to the valley of the energy surface.

Results

Reactant and Product States. QM/MM-optimized reactant and product states were prepared for each of the three main retinal configurations considered here (Figure 1A−C). Schematic representations of the active site in each of the reactant and product states used in the path calculations are given in Figure 2A−F.

A. End States with 13-cis, 14-trans, 15-anti Retinal (Figure 1A). As a result of the constraints used during the refinement procedure, the crystal structure of ref 43, used here to model the 13-cis, 15-anti states, contains a cytoplasmically oriented planar retinal. In the QM/MM-optimized CP−R state (reactant with cytoplasmic-oriented Schiff base, see Figure 2A), the Schiff base region of the retinal is twisted toward Thr89. A hydrogen bonding network extends from the cytoplasmically oriented Schiff base to Asp212 via Thr89, Asp85, and water w402. The existence of an Asp85/Thr89 hydrogen bond prior to proton transfer agrees with conclusions drawn from FTIR spectroscopic data.[68] In the corresponding product state CP−P1 (product with cytoplasmic-oriented Schiff base, see Figure 2B), this hydrogen bond is broken as a result of the displacement toward the extracellular side of the Asp85 protonated side chain. The Schiff base region of the deprotonated retinal is still twisted. The Thr89 hydroxyl group reorients toward the deprotonated Schiff base. No significant protein conformational differences are observed between CP−R and CP−P1.

B. End States with 13,14-dicis, 15-anti Retinal (Figure 1B). The EC−R1 reactant state (extracellular-oriented Schiff base)

(61) Cui, Q.; Elstner, M.; Kaxiras, E.; Frauenheim, T.; Karplus, M. *J. Phys. Chem. B* **2001**, *105*, 569−585.
(62) Zhou, H.; Tajkhorshid, E.; Frauenheim, T.; Suhai, S.; Elstner, M. *Chem. Phys. Lett.* **2002**, *277*, 91−103.
(63) http://www.dl.ac.uk/CFS.
(64) Fischer, S.; Karplus, M. *Chem. Phys. Lett.* **1992**, *194*, 252−261.
(65) Dutzler, R.; Schirmer, T.; Karplus, M.; Fischer, S. *Structure* **2002**, *10*, 1273−1284.
(66) Li, G.; Cui, Q. *J. Phys. Chem. B* **2004**, *108*, 3342−3357.
(67) Choi, C.; Elber, R. J. *Chem. Phys.* **1991**, *94*, 751−760.
(68) Kandori, H.; Yamazaki, Y.; Shichida, Y.; Raap, J.; Lugtenburg, J.; Belenky, M.; Herzfeld, J. *PNAS* **2001**, *98*, 1571−1576.

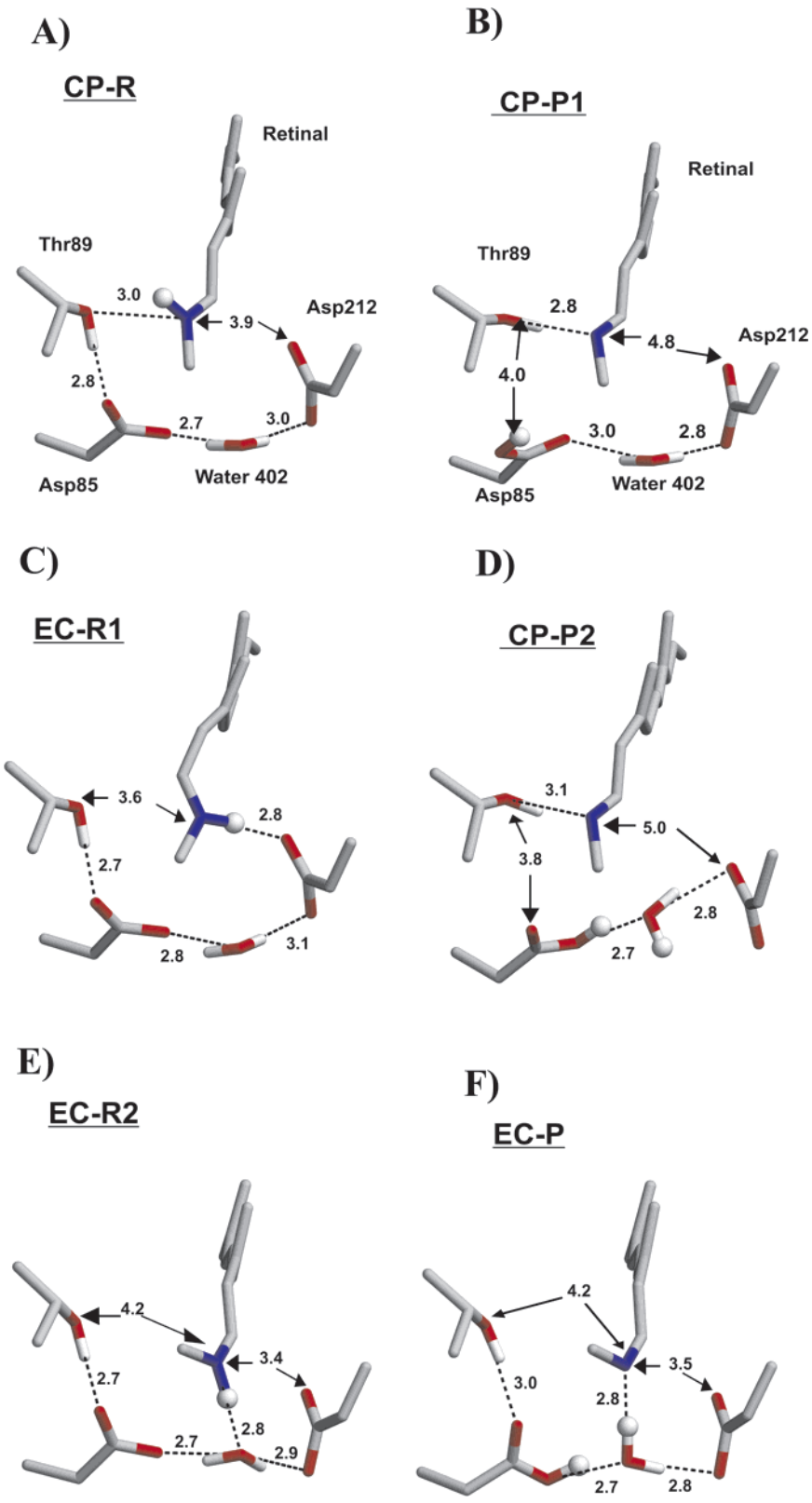

Figure 2. Energy-optimized structures of reactant- and product-state models used in proton-transfer calculations. Cytoplasmic-oriented 13-cis, 14-trans, 15-anti retinal, CP−R (A) and CP−P1 (B); twisted 13,14-dicis retinal in the reactant EC−R1 (C) and its corresponding 13-cis, 14-trans product CP−P2 (D); extracellular oriented 15-syn reactant EC−R2 (E) and product EC−P (F) states.

with retinal in a 13,14-dicis configuration is characterized by a highly twisted retinal hydrogen bonding to Asp212 (Figure 2C). Interestingly, the EC−R1 active-site geometry is similar to that of the twisted 13-cis, 14-trans retinal proposed for the crystal structure K intermediate.[8] The pathway from EC−R1 to CP−R comes over a <2 kcal/mol energy barrier. CP−R is 8.5 kcal/mol lower in energy than EC−R1. The small energy barrier associated with this 13,14-dicis to 13-cis, 14-trans conversion arises from $E^{nb}_{QM/MM}$ (4.5 kcal/mol), while E_{QM} lowers the barrier by 2.1 kcal/mol. The decrease in E_{QM} at the barrier arises

probably from retinal planarization. The lower energy of CP−R as compared to EC−R1 is due mainly to $E^{nb}_{QM/MM}$ (6.4 kcal/mol) and E_{QM} (2.1 kcal/mol).

The rapid possible conversion of EC−R1 to CP−R concurs with molecular dynamics simulations in which the formation of a late KL intermediate was associated with the extracellular-to-cytoplasmic reorientation of the retinal Schiff base.[35] The data presented here would suggest that if a twisted 13,14-dicis forms as a result of photoisomerization (i.e., in K), it may interconvert to 13-cis, 14-trans retinal twisted toward Thr89. As a consequence, to the rate-limiting proton-transfer barrier calculated for 13,14-dicis retinal one must add the 8.5 kcal/mol relative energy between EC−R1 and CP−R.

The Schiff base forms much weaker hydrogen bonds when deprotonated than the protonated. As a result, the 13,14-dicis deprotonated retinal relaxes to a 13-cis cytoplasmic orientation upon energy optimization. The resulting product-state CP−P2 (cytoplasmic-oriented Schiff base, see Figure 2D) is similar to CP−P1. The small differences between the two states concern the position of the acidic proton on Asp85, which is closer to Thr89 in CP−P1 and to water w402 in CP−P2. Thr89 forms a hydrogen bond with the Schiff base. The H−C14−C15−H retinal dihedral angle is −149.9° and −150.6° in CP−P1 and CP−P2, respectively, agreeing well with the experimental value of ±147° (±10°).[69] Moreover, the distance between the C14 retinal atom and Asp212-Cγ is 5.4 Å in CP−P1 and 5.9 Å in CP−P2, close to the value of 4.8 ± 1.0 Å determined by NMR on the M state .[70]

C. End States with 13-cis, 14-trans, 15-syn Retinal (Figure 1C). In the reactant state labeled EC−R2 (extracellular-oriented Schiff base, see Figure 2E) the Schiff base is connected to Asp85 and Asp212 via hydrogen bonds with w402. A hydrogen bond exists between Thr89 and Asp85. The relative positioning of the QM groups does not change much between this state and the extracellular-oriented product state modeled with 13-cis, 15-syn retinal, EC−P (Figure 2F), where the deprotonated Schiff base maintains its extracellular orientation and hydrogen bonds to w402.

Proton-Transfer Pathways. The SCC-DFTB/MM-optimized and B3LYP/MM values for the proton-transfer barriers agree with each other to within 2.0 kcal/mol for the paths investigated here. Unless otherwise specified, all energy values discussed in the text are from SCC-DFTB/MM-optimized pathways. The proton-transfer energy profiles (Figure 3A−D) share several common features. In particular, neutralization of the donor/acceptor charged groups results in a lower energy of the QM fragment, E_{QM}. Another common observation is that the interplay between $E^{nb}_{QM/MM}$ and E_{QM} largely determines the proton transfer energy profiles. In pathways involving extracellular-oriented end states, the MM^{nb} term also contributes to the barrier height.

A. Proton Transfer from CP−R. Cytoplasmically oriented retinal (CP−R, Figure 2A) may deprotonate via a direct pathway that requires significant retinal twisting and simultaneous displacement of the Asp85 side chain (path **1**, Figure 3A). The 12.4 kcal/mol energy barrier (located at $\lambda = 0.36$ in Figure 3A) is due mainly to $E^{nb}_{QM/MM}$ (8.8 kcal/mol), whose impact on the energy barrier is due to the structural rearrangements required to reduce the donor−acceptor distance. The rearrangements taking place in the active site during the pathway induce only small changes in the surrounding MM environment, as indicated by the transition-state values of the MM terms E^{nb}_{MM} (1.7 kcal/mol) and E^{b}_{MM} (1.4 kcal/mol). After proton transfer has completed, E_{QM} and $E^{nb}_{QM/MM}$ undergo variations of opposite sign, such that in CP−P1 E_{QM} is reduced by 5.6 kcal/mol relative to CP−R and $E^{nb}_{QM/MM}$ increased by 11.4 kcal/mol. While at the rate-limiting step $E^{nb}_{QM/MM}$ is almost equally contributed by van der Waals and Coulombic interactions, the larger value of this term in CP−P1 as compared to CP−R arises almost entirely from electrostatic interactions.

B. Proton Transfer from EC−R1. Starting from the 13,14-dicis retinal configuration EC−R1 (Figure 2C), the pathway was calculated for retinal deprotonation via water w402 (path **2**, Figure 3B), as previously suggested.[2,10] This pathway starts with rearrangement of water w402 which, while maintaining a hydrogen bond to Asp85, rotates such that it breaks its hydrogen bond to Asp212 and forms another hydrogen bond to the other Asp212 oxygen (see insets in Figure 3B). Consequently, the Schiff base/Asp212 hydrogen bond breaks and the Schiff base NH group reorients toward w402, reducing to 3.1 Å the initial 3.9 Å distance between the Schiff base and w402. This gives the rate-limiting step of the transfer, with an energy barrier of 5.6 kcal/mol (at $\lambda = 0.17$ in Figure 3B). Further movement of water w402 brings it closer (2.5 Å) to the Schiff base at the second saddle point ($\lambda = 0.33$), whose energy is 3.8 kcal/mol higher than EC−R1. From this configuration proton transfer occurs via w402 in a sequential manner. After proton transfer to Asp85 has completed, retinal cis−trans isomerization around the C14−C15 bond leads to cytoplasmic orientation of the Schiff base.

The rate-limiting barrier is dominated by the opposite-sign contributions of E_{QM} (16.7 kcal/mol) and $E^{nb}_{QM/MM}$ (−12.0 kcal/mol). The significant contribution of E_{QM} arises from breaking of the hydrogen bond between w402 and Asp212 and of the Schiff base/Asp212 salt bridge. After the transfer of the proton to Asp85, E_{QM} and $E^{nb}_{QM/MM}$ reverse sign while remaining antagonistic. That is, relative to the reactant state EC−R1, in the product CP−P2 E_{QM} is reduced and $E^{nb}_{QM/MM}$ increased by 20 kcal/mol and 14.3 kcal/mol, respectively.

The much lower energy barrier of path **2** as compared to path **1** would suggest that the former is preferred. However, the barrier for the interconversion of EC−R1 (the starting state for path **2**) into CP−R is smaller than for the proton-transfer path **2**, indicating that EC−R1 is more likely to proceed with retinal relaxation than with proton transfer. If nevertheless transfer occurs from EC−R1, the rate-limiting proton transfer barrier relative to the lower energy CP−R state is 14.1 kcal/mol, slightly larger than in experiment (∼13 kcal/mol).

C. Proton Transfer from EC−R2. Two proton transfer pathways with barriers of 6−7 kcal/mol were found from EC−R2 (Figure 2E). One of these pathways (path **3a**, Figure 3C), with a barrier of 7.3 kcal/mol, consists of a concerted proton transfer via water 402. In the other pathway (path **3b**, Figure 3D) the proton is directly transferred to Asp85, with a rate-limiting barrier of 5.9 kcal/mol. Only small rearrangements of the active-site groups are observed in these two pathways. The

(69) Lansing, J. C.; Hohwy, M.; Jaroniec, C. P.; Creemers, A. F. L.; Lugtenburg, J.; Herzfeld, J.; Griffin, R. G. *Biochemistry* **2002**, *41*, 431−438.
(70) Griffiths, J. M.; Bennet, A. E.; Engelhard, M.; Siebert, F.; Raap, J.; Lugtenburg, J.; Herzfeld, J.; Griffin, R. G. *Biochemistry* **2000**, *39*, 362−371.

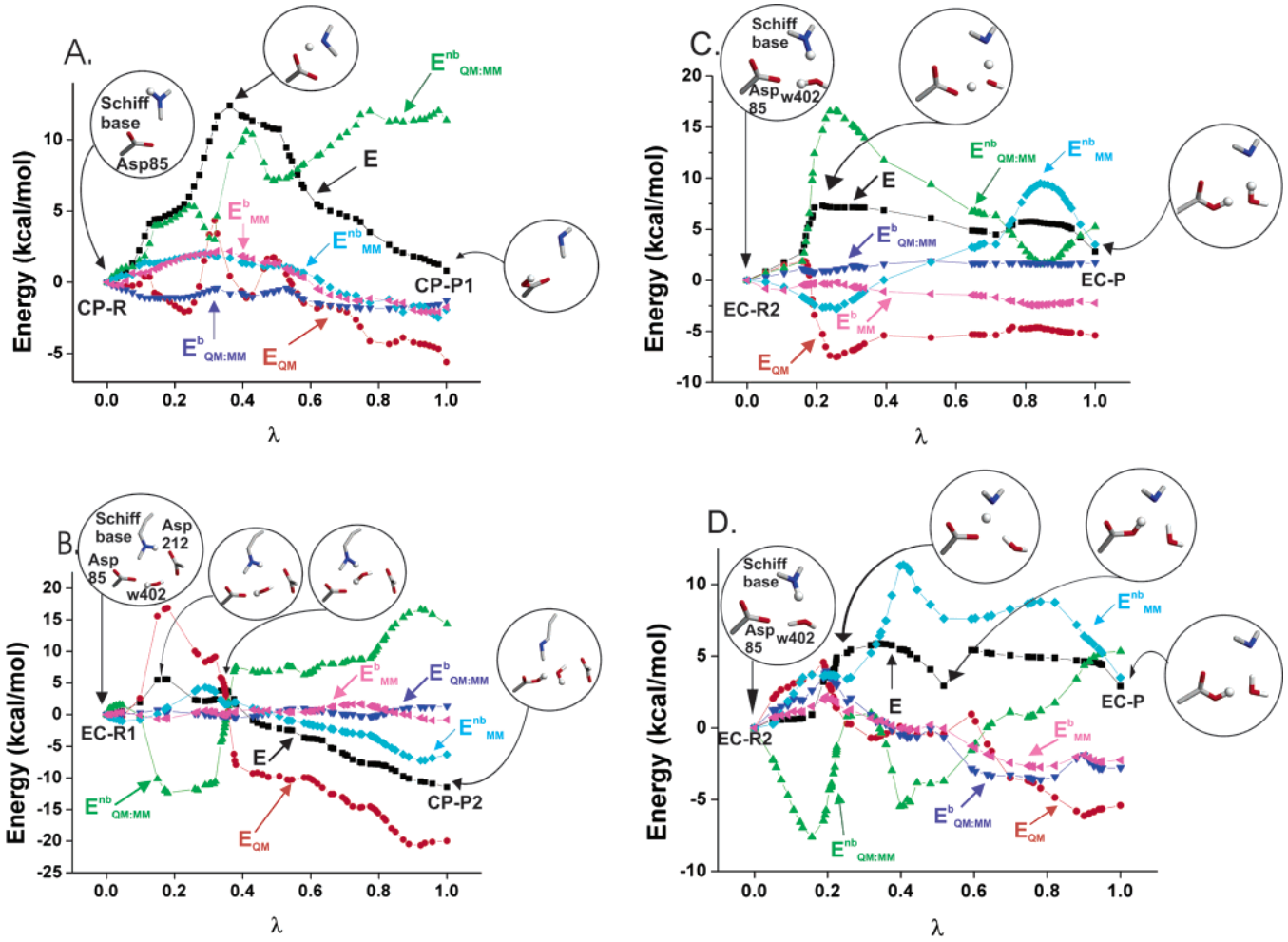

Figure 3. Minimum energy profile of primary proton transfer for the main donor/acceptor orientations. (A) Path **1**, direct proton transfer from CP−R; (B) path **2**, proton transfer via w402 starting from EC−R1; (C) path **3a**, proton transfer via w402 from EC−R2; (D) path **3b**, direct proton transfer from EC−R2. The reaction coordinate λ is the normalized sum along the path of the change in all atomic coordinates measured as an RMS difference.[64] $\lambda = 0$ is CP−R in panel A, EC−R1 in panel B, and EC−R2 in panels C and D. $\lambda = 1$ is the product state CP−P1 in panel A, CP−P2 in panel B, and EC−P in panels C and D. The following colors are used for the energy terms. (Black) total energy, E; (red) interactions between QM particles, E_{QM}; (green) nonbonded interactions between QM and MM subsystems, $E^{nb}_{QM/MM}$; (blue) bonded interactions between QM and MM subsystems, $E^{b}_{QM/MM}$; (light blue) nonbonded interactions between MM atoms, E^{nb}_{MM}; (pink) bonded interactions between MM atoms, E^{b}_{MM}. All energies are SCC-DFTB values taken relative to CP−R in panel A, relative to EC−R1 in panel B, and relative to EC−R2 in panels C,D. The insets show the structure at various points along the path (transferred protons shown as small spheres).

associated barriers have different origins in the two paths, arising mainly from $E^{nb}_{QM/MM}$ in path **3a** (Figure 3C) and from E^{nb}_{MM} in path **3b** (Figure 3D). An increase of E_{QM} prior to proton transfer is observed in both paths **3a** and **3b**. Since in EC−R2 the donor, the acceptor, and the intervening w402 are well oriented for proton transfer via w402 (Figure 2E), in this pathway only a ∼2 kcal/mol increase in E_{QM} is observed (λ = 0.16, Figure 3C). The larger increase of E_{QM} to 4.6 kcal/mol in path **3b** ($\lambda = 0.37$ in Figure 3D) is due to requirement, in order to form a direct path of twisting retinal and reorienting water w402. A feature common to paths **3a** and **3b** is the significant increase in E^{nb}_{MM} after proton transfer has been completed, which may arise from rearrangements of the MM water and protein groups located below the active site (Figures 3C,D). The 2.9 kcal/mol endothermicity observed in paths **3a**,**b** (3.9 kcal/mol at the B3LYP/6-31G** level) arises from electrostatic interactions involving both QM and MM groups.

The 6−7 kcal/mol barrier associated with deprotonation of the 15-syn retinal is much smaller than the experimental enthalpy barrier of ∼13 kcal/mol.[4] However, the endothermicity of the reaction would indicate that proton transfer from the 15-syn intermediate is unlikely to occur. Furthermore, upon deprotonation the 13-cis, 15-syn retinal remains in this configuration, with the Schiff base oriented toward the extracellular side. Reorientation of the Schiff base toward the cytoplasmic side would require rotation around the double bond C_{15}═N associated with an ∼39 kcal/mol torsional barrier.[22] This implies that if proton transfer starts from a 13-cis, 15-syn configuration, the protein will not be able to proceed with the next steps in the photocycle which require reprotonation of the Schiff base from the cytoplasmic side. These energetic considerations lead to the conclusion, in agreement with experiments,[47,71] that during the first proton-transfer step retinal is unlikely to be in a 15-syn configuration. Further support for the incompatibility of the 15-syn retinal with the light-adapted photocycle arises from our investigations on the possible interconversions between retinal pre-proton-transfer configurations. From the analysis of the crystal structures, the twisted 13-cis,15-syn retinal was suggested

(71) Ames, J. B.; Fodor, S. P.; Gebhard, R.; Raap, J.; van der Berg, E. M. M.; Lugtenburg, J.; Matthies, A. *Biochemistry* **1989**, *28*, 3681−3687.

to form from twisted, extracellular oriented 13-cis, 14-trans during the K-to-L transition.[9] This would correspond to a transition from a structure similar to EC−R1 to the modeled EC−R2. Our preliminary QM/MM reaction path calculations indicate that, even though this reaction is significantly exergonic, there is an ∼19 kcal/mol associated rate-limiting barrier, which is too high to be consistent with the experimental ∼1μs time scale of the K-to-L transition.

The possibility cannot be excluded that EC−R2, modeled from the L-state structure of ref 9, corresponds to the dark-adapted state, characterized by a 13-cis, 15-syn retinal: the distance between C_{14} and Trp86N_ϵ is 4.3 Å in EC−R2, as compared to 4.2 Å from solid-state NMR[72] and 4.6 Å from solution state NMR[73] data on the bR dark-adapted state.

Role of the Protein Electrostatic Environment. We have seen above that the proton-transfer pathways are dominated by the interactions among QM atoms and by their Coulombic interactions with the MM protein environment. In path **1**, the increase in $E^{nb}_{QM/MM}$ following proton transfer is not accompanied by significant changes in the MM terms (Figure 3A), implying that this increase originates from the changed geometry and charge distribution of the QM region. The most significant geometry change in the QM region is the displacement of the neutral Asp85 toward the extracellular side. This movement, caused by the repulsion from the Thr89 hydroxyl group, is accompanied by reorientation of the latter toward the deprotonated Schiff base.

Additional calculations were performed to assess the role of the QM geometry and charge distribution on the QM:MM Coulombic interactions. In one calculation on the reactant state CP−R the Schiff base hydrogen was moved to Asp85. Optimization of this hydrogen position was performed keeping the rest of the system fixed. Compared to CP−R the total energy of this neutral system increases by 32.9 kcal/mol, to which E_{QM} contributes 19.9 kcal/mol and $E^{coul}_{QM/MM}$ contributes 12.9 kcal/mol. In a second calculation on CP−R, the whole MM region was kept fixed and the QM system was geometry-optimized for both the zwitterionic (protonated Schiff base, negatively charged Asp85) and neutral (neutral Schiff base and Asp85) configurations. In these calculations the energy of the neutral state was found to be 10.6 kcal/mol higher than the zwitterionic state. The unfavorable energy of the neutral state is due mainly to $E^{coul}_{QM/MM}$ being 8.8 kcal/mol higher in the product than the reactant, whereas E_{QM} has approximately the same value in the zwitterionic and neutral states. In a third calculation a QM/MM optimization was performed, allowing the QM and MM atoms to move (see Methods). The result of this was that in the neutral state CP−P1 E_{QM} is 5.6 kcal/mol lower relative to the zwitterionic CP−R, while $E^{coul}_{QM/MM}$ remains unfavorable by ∼10 kcal/mol. The three calculations above indicate that, while proton transfer lowers the energy of the QM region, it also induces an electrostatic imbalance between this region and the remaining protein environment. The present calculations show that geometrical rearrangements in the retinal region, such as movement of Asp85 toward the extracellular side, contribute to lowering the energy of the neutral relative to the zwitterionic state. Thus, protein flexibility is important for proton transfer. Following proton transfer, longer time scale protein rearrangements may also take place that further relieve the electrostatic conflict between the retinal binding region and the protein environment. However, these longer time scale structural changes are not amenable to the present calculations. Additional support for the existence of these motions arises from test QM/MM calculations indicating that in a post-proton-transfer crystal structure[74] the QM/MM nonbonded interactions favor the neutral state.

Role of Active-Site Protein Groups. The QM residues Thr89 and Asp212 are situated in close proximity to the Schiff base/Asp85 ion pair (see Figure 2). These residues are conserved among bacteriorhodopsins from various halobacteria, suggesting they are important for proton pumping.[75] To investigate the possible role of these residues in retinal deprotonation, additional calculations were performed as follows. Proton transfer energy profiles were calculated for minimal gas-phase systems consisting only of retinal and Asp85 (path **1**, **3b**), or retinal, Asp85, and water w402 (paths **2**, **3a**). Thr89 and Asp212 (and w402 in paths **1**, **3b**) were subsequently added. These subsets of QM atoms were selected from the SCC-DFTB/MM-optimized pathways, and their coordinates among these pathways were conserved. The gas-phase proton transfer energy profiles were computed (without geometry optimization) with SCC-DFTB. The results are presented in Figure 4A−D.

In all minimal models, proton transfer leads to an energy decrease. Consistent with previous reports,[21] the magnitude of this energy decrease depends on the donor/acceptor orientation and on the presence of water. Compared to the zwitterionic state, the neutral state is favored by 12.1 kcal/mol in the case of the extracellular-oriented 13-cis, 15-syn retinal (Figure 4C), by 17.4 kcal/mol in the case of cytoplasmic-oriented 13-cis, 15-anti retinal (black curve in Figure 4A), and by 26.9 kcal/mol in the case of extracellular-oriented 13,14-dicis retinal (black curve in Figure 4B). In the first case (13-cis, 15-syn retinal with the Schiff base pointing toward Asp85), the presence of water w402 contributes to the stability of the zwitterionic state (Figure 4C,D). The stability of the neutral state is consistent with the much higher proton affinity of gas-phase acetate relative to all-trans retinal (∼100 kcal/mol). Addition of Thr89 does not affect the proton-transfer barrier but stabilizes the zwitterionic state by 2.3 kcal/mol (path **3a**, Figure 4C) to 6.4 kcal/mol (path **2**, Figure 4B). The stabilizing role of Thr89 is confirmed by the finding that in the Thr89Val mutant the calculated energy difference between the end states increases by 6.0 kcal/mol relative to the wild type. In other words, the zwitterionic state becomes more unfavored upon removal of the Thr89 hydroxyl group. This concurs with QM/MM results indicating that Thr89 stabilizes the ion pair in the all-trans ground state[34] and with the calculated impact of an active-site threonine residue on the visual rhodopsin ion pair state.[76] Further stabilization of the zwitterionic state arises upon inclusion of Asp212 (green curves in Figure 4A−D). The impact of Asp212 is most significant for the cytoplasmic-oriented retinal in the absence of w402, in which case it

(72) Helmle, M.; Patzelt, H.; Ockenfels, A.; Gärtner, W.; Oesterhelt, D.; Bechinger, B. *Biochemistry* **2000**, *39*, 10066−10071.
(73) Patzelt, H.; Simon, B.; terLaak, A.; Kessler, B.; Kühne, R.; Scmieder, P.; Oesterhelt, D.; Oschkinat, H. *Proc. Natl. Acad. Sci. U.S.A.* **2002**, *99*, 9765−9770.
(74) Sass, H. J.; Büldt, G.; Gessenich, R.; Hehn, D.; Neff, D.; Schlesinger, R.; Berendzen, J.; Ormos, P. *Nature* **2000**, *406*, 649−653.
(75) Brown, L. S. *Biochemistry (Moscow)* **2001**, *66*, 1249−1255.
(76) Sugihara, M.; Buss, V.; Entel, P.; Hafner, J. *J. Phys. Chem. B* **2004**, *108*, 3673−3680.

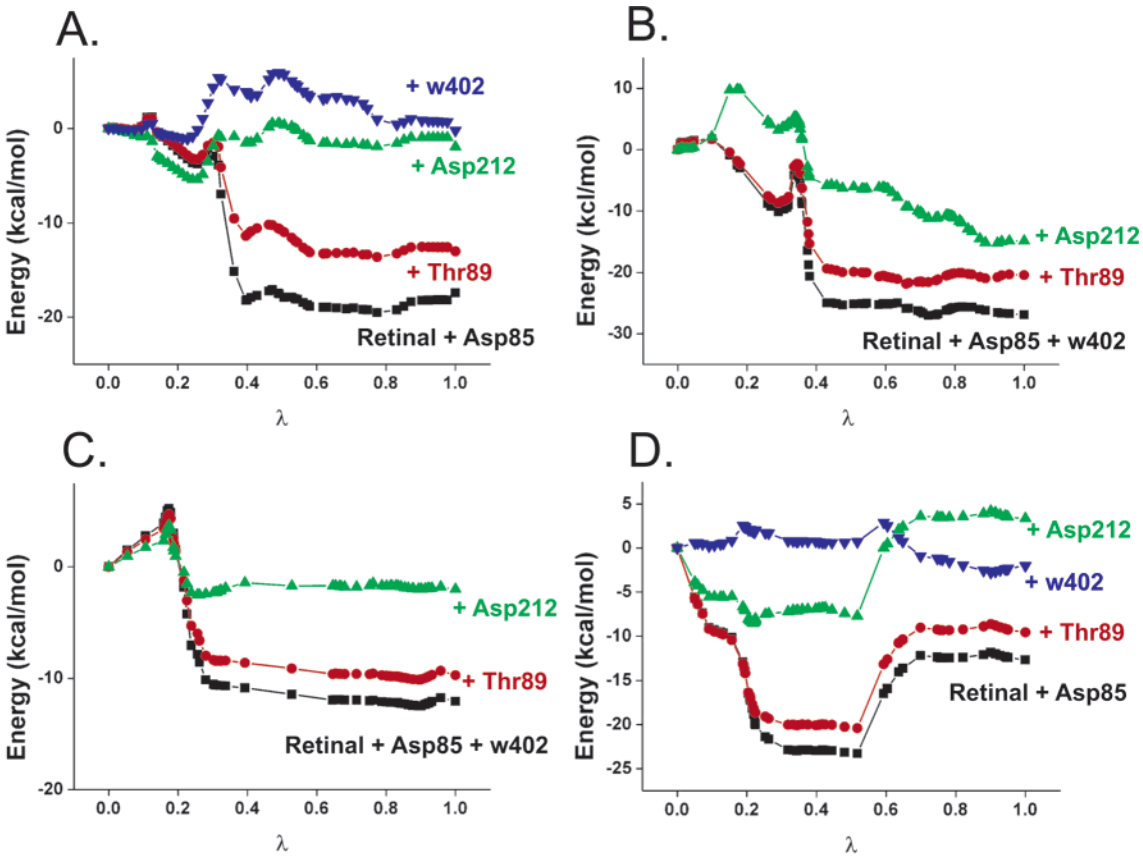

Figure 4. Role of protein active site groups in proton transfer. Panels A to D: same paths as those in Figure 3. The following color codes are used: (black curves) minimal proton-transfer models consisting of retinal and Asp85 (A, D) or retinal Asp85 and w402 (B, C); (red curves) addition of Thr89; (green curves) addition of Asp212; (blue curve) addition of w402 (A, D). Energies are SCC-DFTB values. See Figure 3 for description of λ.

stabilizes the zwitterionic state by ~11 kcal/mol (green curve in Figure 4A).

Given the much higher proton affinity of acetate than retinal, it is expected that proton transfer occurs spontaneously in the minimal gas-phase models. This is indeed observed for paths **1**, **2**, and **3b** (black curves in Figure 4A,B,D) but not for path **3a**, where there is a 5.2 kcal/mol energy barrier (black curve in Figure 4C). In the case of path **2**, breaking and forming of hydrogen bonds between w402 and Asp212 and between the Schiff base and Asp212 lead to the 10 kcal/mol barrier observed when Asp212 is added (green curve in Figure 4B).

Other polar groups surrounding the QM region (e.g., water molecules, tyrosine and tryptophan residues) are also likely to have an impact on the energy profile. Moreover, Arg82, an amino acid residue that is part of the extracellular proton release group, has a significant impact on the proton transfer from the retinal Schiff base when extracellularly oriented. For example, when the Arg82 partial charge is switched off, the barrier for path **3b** increases by 3.6 kcal/mol. For cytoplasmically oriented retinal, the effect is much smaller (1 kcal/mol for path **1**).

Conclusions

Retinal protonation and deprotonation is part of the proton-pumping photocycle of bacteriorhodopsin. In visual and sensory rhodopsins, deprotonated retinal is associated with the signaling state. Accordingly, control of the protonation state of their chromophore is a major issue in the function of retinal proteins. The electrostatic environment of these proteins is adjusted such that the transfer of the Schiff base proton to a nearby carboxylate is an activated process. In the particular case of bacteriorhodopsin, proton transfer does not take place before retinal photoisomerization even though the proton donor and acceptor groups are connected through hydrogen bonds to water 402. For proton transfer to take place retinal must first photoisomerize, leading to a specific geometry of the binding site.[15,21,77]

Both the barrier height and the relative energies of the zwitterionic and neutral states are crucial for the primary proton-transfer activity. Also important is the capacity of retinal to orient its deprotonated Schiff base toward the cytoplasmic side, such that it can be reprotonated from Asp96 at a later stage in the photocycle. The present calculations suggest that this reorientation cannot be achieved when deprotonation occurs from a 13-cis, 15-syn retinal configuration. Consequently, consistent with experimental findings,[47,71] the 13-cis, 15-syn configuration cannot be the state accumulating prior to proton transfer. The protein avoids the unproductive 13-cis, 15-syn deprotonated retinal states by rendering unlikely the formation of 13-cis, 15-syn photointermediates[78] and their deprotonation.

The 13-cis, 15-anti retinal appears to be compatible with the photocycle regardless of the isomeric state around the 14−15 bond. The 13,14-dicis retinal is significantly higher in energy, and it is more likely to relax to a 13-cis, 14-trans configuration than to proceed with proton transfer.

(77) Sheves, M.; Albeck, A.; Friedman, N.; Ottolenghi, M. *Proc. Natl. Acad. Sci. U.S.A.* **1986**, *83*, 3262−3266.
(78) Orlandi, G.; Schulten, K. *Chem. Phys. Lett.* **1979**, *64*, 370−374.

The configuration of the 13-cis, 14-trans cytoplasmic-oriented retinal found by our QM/MM calculations is similar to that indicated by an L-state crystal structure that became available after completion of this work.[79] However, an important difference between these two structures is the position of water w402. Based on the interpretation of electron density changes, in ref 79 it was proposed that during the K-to-L transition water w402 translocates from below to above the retinal Schiff base and further moves to the intracellular side during the L-to-M transition. This interesting proposal concurs with recent observations on the dynamics of internal water molecules from FTIR[80] and from QM/MM proton-transfer[37] and molecular dynamics[35] calculations. Our preliminary QM/MM pathway calculations (not shown) indicate a high-energy barrier (∼15 kcal/mol) associated with this water translocation, inconsistent with the experimental microsecond time scale for the rise of L. However, the possibility cannot be excluded that in the L intermediate a cytoplasmic water molecule becomes more ordered, while w402 becomes more disordered. When water w402 is absent, the cytoplasmic-oriented retinal can easily deprotonate over a 6.3 kcal/mol energy barrier, much lower than the experimental value. The fact that in the absence of water w402 proton transfer occurs much faster than the experimental time scale is consistent with the presence of water w402 during proton transfer.

Detailed energy decomposition of the proton-transfer energy profiles has allowed quantification of the opposite-sign effects of the Asp85/retinal interaction and the interaction between these two groups with the protein electrostatic environment. The key role of the protein electrostatic interactions for the bacteriorhodopsin proton transfer detailed here is consistent with the concepts that electrostatic effects are crucial for enzymatic catalysis[33,81] and may control the reactions of retinal proteins.[18,82] The stability of the ion pair state in bacteriorhodopsin depends partly on the configuration of the retinal, which determines specific relative orientations of the proton donor and acceptor groups and partly on electrostatic interactions with the active-site groups Thr89, Asp212, and w402 (which themselves also depend on the retinal configuration).

The results presented here suggest a qualitative model for the mechanism by which bacteriorhodopsin controls retinal deprotonation. In this model, just prior to the first proton-transfer step the electrostatic environment acting on the retinal region is not very different from that in the nonisomerized, bR state, in which the stabilization of the zwitterionic state may be achieved through a preorganized protein electrostatic environment.[83] Indeed, spectroscopic data indicate that no significant conformational changes take place in the first half of the photocycle.[1,49,50] As a result of retinal photoisomerization the interactions of the donor and acceptor groups with the preorganized protein environment changes such that neutralization of the donor/acceptor pair becomes energetically favorable. This requires a certain degree of protein flexibility but nevertheless occurs faster than the protein can adapt its conformation to the new charge distribution. Consequently, an electrostatic conflict arises between the retinal Schiff base region and the rest of the protein. The possibility exists that the subsequent larger-scale conformational changes that occur after retinal deprotonation[1] are induced by the electrostatic conflict revealed here. Further calculations will be performed to investigate this hypothesis. Molecular movies of some transfer paths[86] are downloadable from http://www.iwr.uni-heidelberg.de/groups/biocomp/fischer/ .MolScript2.1.2[84] and Povray3.1g[85] were used in preparing Figures 2 and 3.

Acknowledgment. This work was supported by the Deutsches Krebsforschungszentrum Heidelberg, the Deutsche Forschungsgemeinschaft (SM 63/7), and the Human Frontier Science Program (RG0229/2000-M). The calculations were performed using the Deutsches Krebsforshungszentrum and the IWR, University of Heidelberg computer facilities. N.B. wishes to thank Dr. Matthias Ullmann and Dr. Dan Mihailescu for fruitful discussions and Torsten Becker for comments on an early version of the manuscript. We thank Dr. Jérôme Baudry for providing retinal topology and parameter files.

JA047982I

(79) Kouyama, T.; Nishikawa, T.; Tokuhisa, T.; Okumura, H. *J. Mol. Biol*. **2004**, *335*, 531−546.
(80) Maeda, A.; Herzfeld, J.; Belenky, M.; Needleman, R.; Gennis, R. B.; Balashov, S. P.; Ebrey, T. G. *Biochemistry* **2003**, *42*, 14122−14129.
(81) Villa, J.; Warshel, A. *J. Phys. Chem. B.* **2001**, *105*, 7887−7907.
(82) Warshel, A. *Proc. Natl. Acad. Sci. U.S.A.* **1978**, *75*, 2558−2562.
(83) Koutalos, Y.; Ebrey, T. G.; Gilson, H. R.; Honig, B. *Biophys. J*. **1992**, *58*, 493−501.
(84) Kraulis, P. J. *J. Appl. Crystallogr*. **1991**, *24*, 946−950.
(85) http://www.povray.org.
(86) (86) Bondar, A.-N.; Elstner, M.; Suhai, S.; Smith, J. C.; Fischer, S. *Structure* **2004**, *12*, 1281−1288.